Applied Surface Science 609 (2023) 155380

Contents lists available at ScienceDirect

Applied Surface Science

journal homepage: www.elsevier.com/locate/apsusc

Full Length Article

The effect of cross-linker structure on interfacial interactions, polymer dynamics and network composition in an epoxy-amine resin

Suzanne Morsch [a,1,*], Charlie R. Wand [b,c,1], Simon Gibbon [a], Mark Irwin [d], Flor Siperstein [b], Stuart Lyon [a]

[a] Corrosion and Protection Centre, Department of Materials, The University of Manchester, The Mill, Sackville St, Manchester M13 9PL, UK
[b] Department of Chemical Engineering, The University of Manchester, The Mill, Sackville St, Manchester M13 9PL, UK
[c] Natural Sciences, College of Engineering, Mathematics and Physical Science, Harrison Building, Streatham Campus, University of Exeter, North Park Road, Exeter EX4 4QF, UK
[d] AkzoNobel Powder Coatings, Stoneygate Lane, Felling, Gateshead, Tyne & Wear NE10 0JY, UK

ARTICLE INFO

Keywords:
Iron-oxide
Epoxy-amine
Interface
ATR-FTIR
Molecular dynamics simulation

ABSTRACT

Understanding interactions at the polymer / metal oxide interface is central to improving the performance lifetime of corrosion resistant coatings, where network polymers commonly form via step growth mechanisms in the presence of pigments. Here we employ a holistic analytical approach encompassing ATR-FTIR, DSC and molecular dynamics simulations to consider how crosslinker structure affects adsorption and incorporation into the network, using a stoichiometric mixture of diglycidylether of bisphenol-A (DGEBA) with m-xylylenediamine (MXDA) cured in the presence of hematite (Fe_2O_3) and goethite (FeOOH) powders. We find that the rigid MXDA molecule has two distinct binding modes on both hematite and goethite, and that synergistic hydrogen bonding modes observed on goethite limit interconversion between the two. Moreover, we find that binding persists in fully cured composite samples, determining the levels of residual amine. In contrast to previously reported results using triethylenetetramine (TETA) crosslinkers, however, we find that the Tg of composite specimens is independent of added hematite and goethite volumes. Molecular dynamics simulations demonstrate this is due to electrostatic binding between the cationic Fe sites and electronegative heteroatoms in MXDA. This renders both amine functionalities unavailable for incorporation into the network and hence, unlike TETA, MXDA adsorption does not determine polymer dynamics.

1. Introduction

Epoxy-amine resins are widely used as protective coatings, structural adhesives, and in advanced composites due to their favourable mechanical properties and good heat and chemical resistance. In these applications, the interactions between the epoxy-amine resin and an inorganic solid surface are critical in determining the performance. These interactions may occur prior to, during and following the polymerisation reaction (or cure), which occurs via a step growth mechanism. This leads to the formation of a structurally distinct interphase region [1,2] which is widely considered to be a critical factor in determining the performance; e.g. surface adhesion [3], fracture toughness [4,5] and the leaching of active pigments in protective coatings [6]. Therefore, a comprehensive understanding of the interfacial interactions in epoxy-amine resins and other network polymer systems has been a long-standing goal of material scientists. The buried nature of this interface and the nanoscale dimensions of interphase regions have, however, meant that it is still an open question.

Experimental characterisation of the buried interface and interphase regions in resins has been hampered by the sensitivity and resolution of available organic analysis techniques, many of which are destructive. Historically, the structure of the epoxy-amine interphase regions has typically been inferred based on thermal analysis and spectroscopic investigation of thin films [7,8,9,4,10,11]. It has however, recently been demonstrated that thin films do not accurately represent epoxy-amine interphase regions [5,12,13]. The extent of under-curing is frequently over-estimated, because specimen preparation is problematic; molecular amine constituents may be lost to oxidation, carbamation or evaporation

* Corresponding author at: Department of Materials, The University of Manchester, The Mill, Sackville St, Manchester, M13 9PL (S. Morsch).
E-mail addresses: suzanne.morsch@manchester.ac.uk (S. Morsch), c.wand@exeter.ac.uk (C.R. Wand).
[1] S.M and C.R.W contributed equally to this paper.

https://doi.org/10.1016/j.apsusc.2022.155380
Received 10 August 2022; Received in revised form 4 October 2022; Accepted 17 October 2022
Available online 21 October 2022

upon application. Furthermore, for thin films, increasing contributions of the polymer-air interphase may prevent accurate interpretation. Separately, the nature of molecular binding to metal-oxide interfaces has been explored using X-ray photoelectron spectroscopy (XPS) for individual epoxy and amine molecules [14,15]. Whilst this approach can yield detailed insights into the interfacial binding mode, the influence of molecular adsorption on network formation cannot be assessed in this manner. Recently however, detailed analysis of nanocomposites, i.e., specimens containing large areas of metal-oxide interface, has demonstrated that the physicochemical properties of the buried polymeric interphase can successfully be inferred via conventional analysis of macroscopic specimens, providing a promising alternative to thin film experiments [16,17].

At the same time, computer simulations have emerged as a promising route to investigate the buried interface, particularly when used in conjunction with experimental analysis methods. Quantum mechanical calculations have been performed to investigate the adsorption of epoxy-amine systems to alumina, iron, and iron oxide surfaces [18–22]. However, due to the computational cost, such calculations can only be applied to small systems on the order of tens of atoms. Classical molecular dynamics (MD) simulations can extend the system size to the nanoscale but lack the ability to accurately capture bond formation. Bahlakeh et al combine the two approaches and find good agreement for an epoxy-amine system on iron oxide surfaces, due to the lack of chemical bond formation formed between the epoxy-amine and the surface [23]. Lee et al also found that chemisorption does not occur for an epoxy precursor on an iron or iron oxide surface. This lack of bond formation on iron oxide surfaces makes it ideally suited for classical MD simulations [22]. We recently reported a holistic approach combining MD simulations, AFM-IR, FTIR and DSC techniques to investigate the formation of interphase regions in diglycidyl ether of bisphenol-A (DGEBA) and triethylenetetraamine (TETA) epoxy-amine resins at iron oxide interfaces [16]. Molecular dynamics simulations revealed strong interfacial binding through amine or hydroxy functionalities of the resin constituents to specific surface sites on goethite. The position of surface hydroxy protons on goethite was found to engender synergistic hydrogen bonding and electrostatic binding to Fe atoms at specific sites. This newly identified binding mode provides a strong driving force for molecular orientation, and therefore restricted segmental motion.

To predict the nature of interfacial binding on iron oxides and the development of interphase regions in coatings, further investigations involving alternative chemical structures are needed. In light of this, in the present study m-xylylenediamine (MXDA) was selected as a representative aralkylamine curing agent, commonly used in coating formulations to confer efficient low temperature curing and improve thermo-mechanical properties of epoxy network polymers due to its limited molecular flexibility [24,25]. We apply molecular dynamics simulations alongside conventional infrared and thermal analysis of composite specimens prepared using DGEBA to investigate the binding of MXDA to goethite and hematite iron oxide surfaces, and its effect on network polymer interphase properties.

2. Experimental

2.1. Composite sample preparation

Epoxy-amine resins consisted of stoichiometric mixtures of diglycidyl ether of bisphenol-A (DGEBA) epoxy (D.E.R. 332, Sigma, used as received) and m-xylylenediamine (MXDA) hardener (99 %, Sigma, used as received), Scheme 1. Pre-weighed iron oxide pigment powders were dispersed in the epoxy component using a dual axis centrifuge operating at 2500 rpm (Speedmixer, Flacktek Inc.) before the addition of the amine cross-linker and further mixing at 1500 rpm, to achieve final pigment volume concentrations between 0.5 % and 3.5 %. The pigments investigated were Bayferrox 140 M (>94 % synthetic Fe_2O_3, Bayer), and Bayferrox 3920 (>99 % synthetic Fe(O)OH, Bayer). We have previously

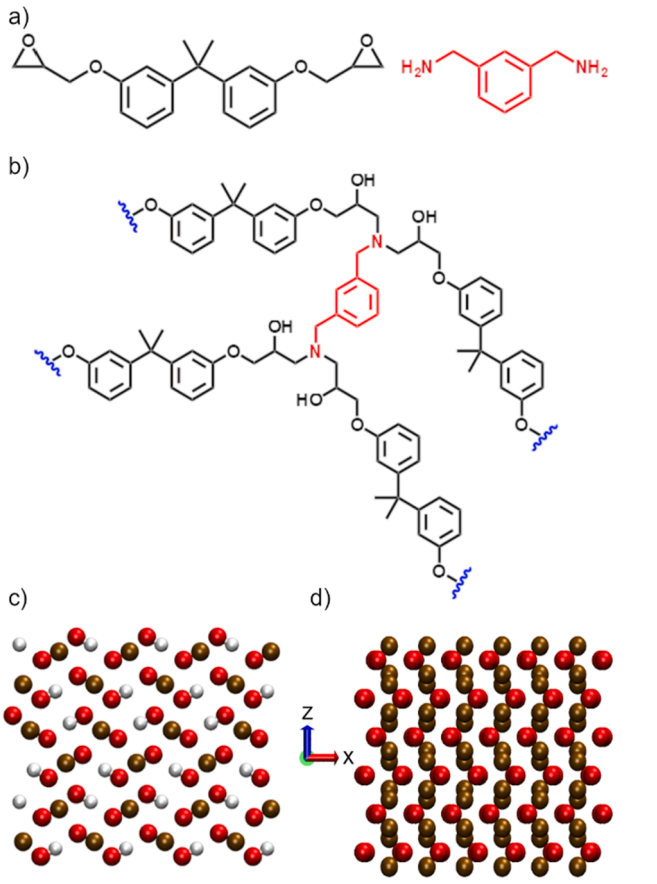

Scheme 1. (a) Diglycidyl ether of bisphenol-A (DGEBA) epoxy and m-xylylenediamine (MXDA); (b) the cross-linking reaction product of DGEBA and MXDA; (c) goethite surface and (d) hematite surface. The red, white and brown spheres correspond to oxygen, hydrogen, and iron respectively.

reported SEM derived dimensions of these pigments as follows: 210 nm ± 90 nm and 250 nm ± 110 nm diameters for globular magnetite and hematite particles respectively, whilst acicular goethite pigments measured 420 ± 190 nm in length and 80 nm ± 10 nm in width [16]. Note that although pigments are referred to as iron oxides throughout for simplicity, Fe(O)OH is an iron oxyhydroxide. Composites were allowed to cure under ambient temperature (22 °C), in a convection oven maintained at 50 °C or in a convection oven at 120 °C for 7 days, before post-cure heating at 120 °C for 2 h. In order to expose the bulk structure, composite specimens were sequentially abraded using 600, 800 and 1200 grit silicon carbide grinding papers, with water as a lubricant. Samples were then thoroughly rinsed in deionised water, air dried and stored in a desiccator prior to analysis.

3. Fourier Transform Infrared (FTIR) spectroscopy

ATR (attenuated total reflection)-FTIR (Fourier Transform Infrared) spectroscopy of the composite epoxy-amine / iron oxide specimens was performed using a FTIR-spectrometer (Nicolet 5700 spectrometer, Thermo Electron Corp.) equipped with room-temperature DTGS (deuterated triglycine sulfate) detector operating at 4 cm^{-1} resolution across the 4000–500 cm^{-1} range. 64 co-averages were added to every spectrum. Backgrounds (in air) were collected prior to each spectrum.

3.1. Dynamic Scanning Calorimetry (DSC)

For DSC measurements, 6–10 mg specimens were placed in closed aluminium pans. DSC thermograms were obtained using a heat-cool-heat cycle over a temperature range of 0–200 °C under nitrogen, using

a heating / cooling rate of 10 °C min^{-1}/5 °C min^{-1} (Q100 DSC, TA Instruments).

3.2. Molecular dynamics simulations

Molecular dynamics simulations were used to investigate the binding energy, ΔE_{bind}, of a single m-xylylenediamine (MXDA) molecule to hematite and goethite surfaces.[26] The binding energy is defined as

$$\Delta E_{bind} = E_{adsorbate/surface} - \left(E_{adsorbate} + E_{surface}\right) \quad (1)$$

where $E_{adsorbate}$ and $E_{surface}$ are the potential energy of the adsorbate and surface in vacuum and $E_{adsorbate/surface}$ is the potential energy of the adsorbate on the surface. Simulations were run at constant number of particles, volume, and temperature (*NVT*) using LAMMPS (the Large-scale Atomic/Molecular Massively Parallel Simulator) [27]. A Nosé-Hoover thermostat [28] is used to control the system temperature and a standard velocity-Verlet [29] algorithm to integrate through time with a time step of 2 fs. Periodic boundary conditions are used in three dimensions and the long-range electrostatic forces are handled using a standard particle–particle–particle-mesh (PPPM) solver [30].

The surfaces were generated by replicating the crystallographic information along three Cartesian coordinates to form a crystalline slab with a surface normal to the *z* direction. In this work, we consider the (0001) surface for hematite and the (1 0 0) surface goethite, which are the most thermodynamically stable [31,32]. Note that here we use the *Pnma* space group for goethite. The simulation box was approximately 80 Å in the directions parallel to the surface (*x,y*) and 200 Å in the direction normal to the surface (*z*) to avoid interactions with its periodic images. The surfaces were represented using the CLAYFF force field [33] with the modification suggested by Kerisit [34] to account for octahedrally coordinated iron. The surface is held rigid throughout the simulations, that is, that the atoms in the surface were not integrated through time. Therefore, the *intra*-slab interactions are not considered within this work. Also note that here we only consider an atomically smooth surface whilst in reality there will be lower coordination sites at edges and corners, however these are beyond the scope of this paper.

The MXDA adsorbate molecule is represented using the Optimized Potentials for Liquid Simulations (OPLS-AA) force field [16] and the C—H bonds were constrained using the SHAKE algorithm [35]. The charges were calculated using the 1.14*CM1A [36] in LigParGen [37] and averaged over equivalent sites. More details can be found in the supporting information. In all cases the cross interactions were accounted for using standard Lorentz-Berthelot mixing rules and a cut-off of 10 Å was used. The starting configurations were prepared using Moltemplate [38], with the MXDA placed approximately 25 Å away from the surface. Atoms within MXDA were assigned initial velocities from a Gaussian distribution with a mean of 0.0 and a standard deviation to produce the average temperature of 300 K, with zero linear momentum. The system was then run for a total of 8 ns, consisting of a 4 ns equilibration run and a 4 ns production run. A total of 10 independent runs are used for both surfaces.

Alongside the binding energy, the simulations were analysed by calculating the average distance between the nitrogen atoms in MXDA, $|r_{N-N}|$, and the distance between the centre of the aromatic ring and the surface, $|r_{Aro-surface}|$ and the radial distribution function (rdf). These properties were averaged over the entire production run, using configurations taken every 100 ps. The analysis was carried out using a combination of MDAnalysis [39,40] and in house codes.

4. Results

4.1. Infrared spectroscopy

The influence of added iron oxide content on the chemical structure of DGEBA-MXDA network polymers was initially investigated using infrared spectroscopy. The overall cure degree of the polymer binder in composite specimens cured under ambient temperature, at 50 °C and at 120 °C was assessed using the band at 1105 cm^{-1} corresponding to the out of phase C—C—O stretch for secondary alkyl hydroxy groups generated by the epoxy-amine reaction, Scheme 1 and Fig. 1 [41–43]. Integration of this band, and normalisation to the area of the aromatic band at 1504 cm^{-1}, demonstrated that under ambient temperature the reaction is retarded in the presence of hematite and goethite, and hence fewer secondary hydroxy groups are created, Fig. 2. This is consistent with our previous observations for DGEBA-TETA iron oxide composites and can be ascribed to entropic segregation of the more mobile amine molecules prior to the cross-linking reaction.[16] Indeed, when elevated cure temperatures were employed, the correlation of secondary hydroxy groups to iron oxide content disappears, indicating that the enhanced mobility of molecules at higher temperature counteracts entropic segregation effects. Note that, whilst previously reported AFM-IR analysis for TETA systems demonstrated that under-curing in this manner is localised to the iron oxide particles, chemical gradients lay beyond the resolution limits of the technique, thus the under-developed region formed as a result of entropic segregation could only be said to be limited to <50 nm in depth [16]. Furthermore, since particles are of an irregular shape, the expected volume of under-developed polymer in these systems cannot be defined.

The use of MXDA as a cross-linker allowed the concentration of residual unbound amine in composite specimens to be compared directly, via integration of a characteristic band identified at 696 cm^{-1}, corresponding the C—N—H wag of the primary amine (note that this is a very strong band in the MXDA infrared spectrum), Fig. 1. Since this band is not overlapped by any DGEBA absorbance peaks, it provides a sensitive measure of unreacted amine content, which is anticipated in stoichiometric formulations, since the reaction is not perfectly selective and a minor degree of epoxy homopolymerization will occur [42]. Here, integration of the 696 cm^{-1} amine band and normalisation to the area of the aromatic band at 1504 cm^{-1} showed that as the volume of hematite or goethite iron oxide was increased, a decreasing amount of residual amine remained after curing under ambient temperature, Fig. 3. Note that, if this amine depletion was a consequence of reaction with epoxy functionality, then secondary hydroxy group concentrations would be expected to increase accordingly, and this is not the case. Furthermore, purely entropic segregation of the amine, in the absence of any surface binding, would be expected to result in an increased concentration of

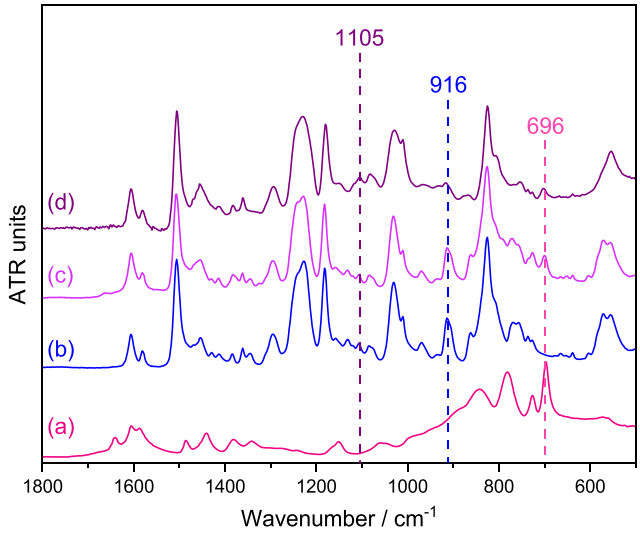

Fig. 1. ATR-FTIR fingerprint region spectra of (a) MXDA; (b) DGEBA; (c) a stoichiometric mixture of MXDA and DGEBA 1 h after mixing and storage under ambient temperature and (d) after 7 days curing under ambient temperature and 24 h post cure heating at 120 °C.

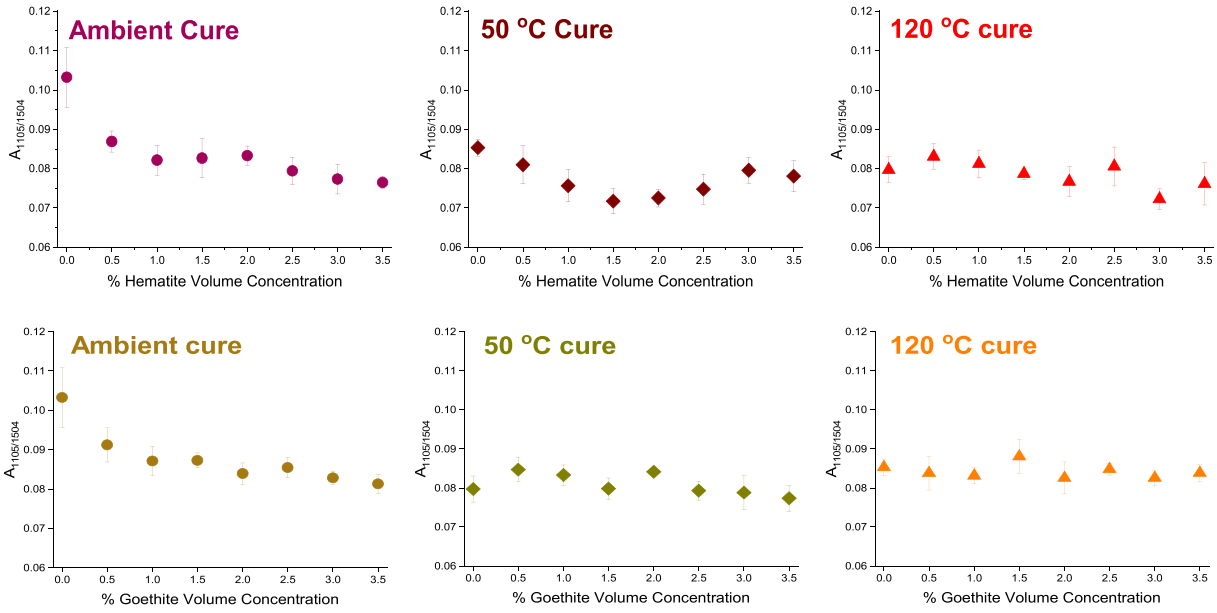

Fig. 2. Normalized areas of the secondary hydroxy band at 1105 cm^{-1} as a function of added hematite (top) and goethite (bottom) volume concentrations in DGEBA-MXDA polymer cured under ambient temperature (left) at 50 °C (middle) and 120 °C (right). Points correspond to the mean of five measurements and error bars correspond to the standard deviation.

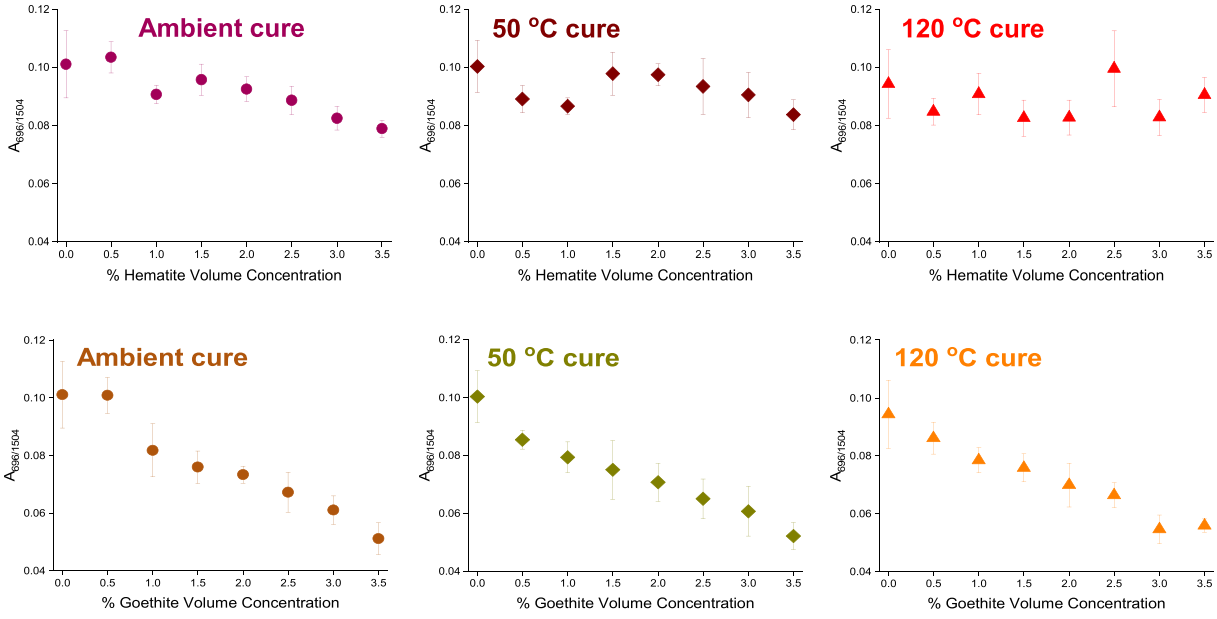

Fig. 3. Normalized areas of the residual primary amine band at 696 cm^{-1} as a function of added hematite (top) and goethite (bottom) volume concentrations in DGEBA-MXDA polymer cured under ambient temperature (left) at 50 °C (middle) and 120 °C (right). Points correspond to the mean of five measurements and error bars correspond to the standard deviation.

unreacted residual amine. The observed trend is therefore attributed to amine depletion as a result of binding to the surface of iron oxide particles (since binding will restrict C—N—H wagging vibrations, and hence shift the infrared absorbance frequency). For hematite composites, the correlation between added pigment and residual amine disappears when the cure reaction is performed at 120 °C. Conversely, in the case of goethite, the correlation persists after reaction at elevated temperatures, indicating that the amine is strongly bound.

Finally, no clear correlation could be detected between the area of the weak epoxy band at 916 cm^{-1} (asymmetric oxirane ring deformation) after normalization to the area of the aromatic band at 1504 cm^{-1} and hematite volume concentration (this band is overlapped by FeOOH bands for goethite composites), Fig. 4. It should, however, be noted that this band is extremely weak in the composites studied here, which were subjected to longer curing prior to analysis than previously reported DGEBA-TETA composites (7 days vs 1 day). In addition, the lower overall concentrations of secondary hydroxy groups and residual epoxy following 120 °C curing is indicative of an increased contribution of epoxy homopolymerization reactions (epoxy-hydroxy reaction) at high temperatures [41].

4.2. Thermal analysis

DSC analysis shows that neither the cure temperature, nor the

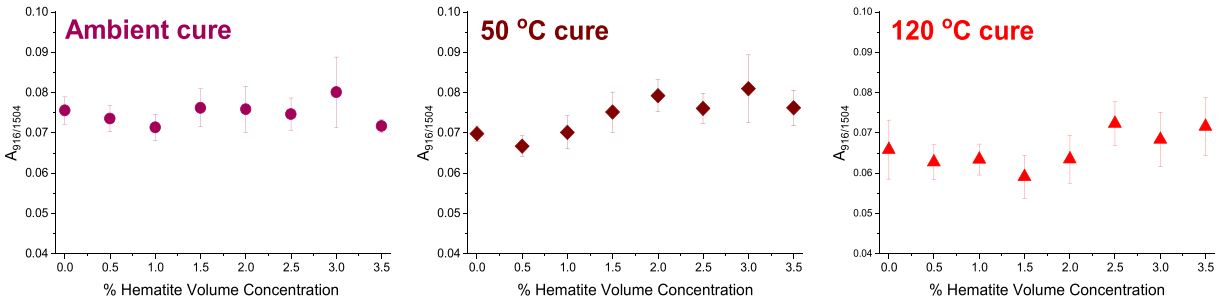

Fig. 4. Normalized areas of the residual epoxy band at 916 cm^{-1} as a function of added hematite volume concentrations in DGEBA-MXDA polymer cured under ambient temperature (left) at 50 °C (middle) and 120 °C (right). Points correspond to the mean of five measurements and error bars correspond to the standard deviation.

addition of hematite or goethite powder has any effect on the measured Tg values of DGEBA-MXDA resins, Fig. 5. This indicates that the minor stoichiometric shifts detected using FTIR do not result in significant changes to the overall cross-linking density, and that the reaction can in all cases be considered complete. These results are however, somewhat surprising given that infrared data indicates strong binding between MXDA and goethite. In a previous study, we demonstrated that strong binding between a DGEBA-TETA network polymer and the goethite interface restricts segmental motion, resulting in raised Tg values for composite specimens containing comparable volumes of goethite powder (represented by crosses in Fig. 5) [16].

4.3. Molecular dynamics simulations of interfacial interactions

In order to understand the experimental data, detailed insights into amine adsorption onto hematite and goethite interfaces were sought using molecular dynamics simulations. Surprisingly, given that amine adsorption persists at high temperatures on goethite, we find that the binding energy, ΔE_{bind}, is more favourable for MXDA on hematite than goethite, with the mean ΔE_{bind} of −54.2 and −27.6 kcal mol^{-1} respectively. These values are, however, consistent with results we have obtained previously for DGEBA, triethylenetetramine (TETA), and methyl diethanolamine (MDEA) on both surfaces [16]. On hematite we have previously attributed the primary interaction for the adsorption to the electrostatic interactions between the electronegative heteroatoms and δ + Fe sites. ΔE_{bind} is around 10 kcal mol^{-1} higher (i.e., less favourable) for MXDA on hematite than for TETA on hematite due to the decreased number of heteroatoms, with MXDA possessing two primary amines whilst TETA contains two secondary amines alongside two primary amines. For the goethite surface, ΔE_{bind} for MXDA, TETA and MDEA are much more similar due to the formation of synergistic hydrogen bonds between the adsorbate heteroatoms and the surface hydroxy groups that cause the adsorbate molecules to form a "bridging" configuration where only the terminal heteroatoms interact strongly with the surface.

In the case of MXDA over the repeated runs we found two distinct ΔE_{bind} values for both surfaces with an energy difference of approximately 4–7 kcal mol^{-1}, corresponding to an 11 % and 14 % difference for hematite and goethite respectively (Fig. 6). We attribute these two stable modes found for MXDA to the increased rigidity of the molecule in comparison to the previous crosslinker investigated (Fig. 7).

We use a variety of intra- and inter- molecular distances to fully characterise the two low energy binding modes. To do this we have defined two representative distances, the distance between the two nitrogen atoms in MXDA, $|r_{N-N}|$, and the distance between the centre of the aromatic ring and the surface of the substrate, $|r_{Aro-surface}|$. The two distinct modes can be distinguished by either of these distances. On both surfaces, the shorter $|r_{N-N}|$ corresponds to a longer $|r_{Aro-surface}|$ (Figs. 7 and 8). The rigid nature of MXDA means that by increasing the separation between amine groups, the aromatic ring is forced into a more upright position, away from the surface. On average $|r_{Aro-surface}|$ is 4.4 Å on goethite and 2.9 Å on hematite. We attribute the longer $|r_{Aro-surface}|$ on goethite due to the definition of the surface which is defined as the position of the top δ + Fe site. On goethite there is a hydroxy group above the reference Fe site which restricts the distance that the MXDA can approach. The oxygen sits at 0.93 Å above the Fe site, taking this into account the modified distance $|r'_{Aro-surface}|$ on goethite is 3.47 Å, which is still significantly larger than the separation on hematite, due to

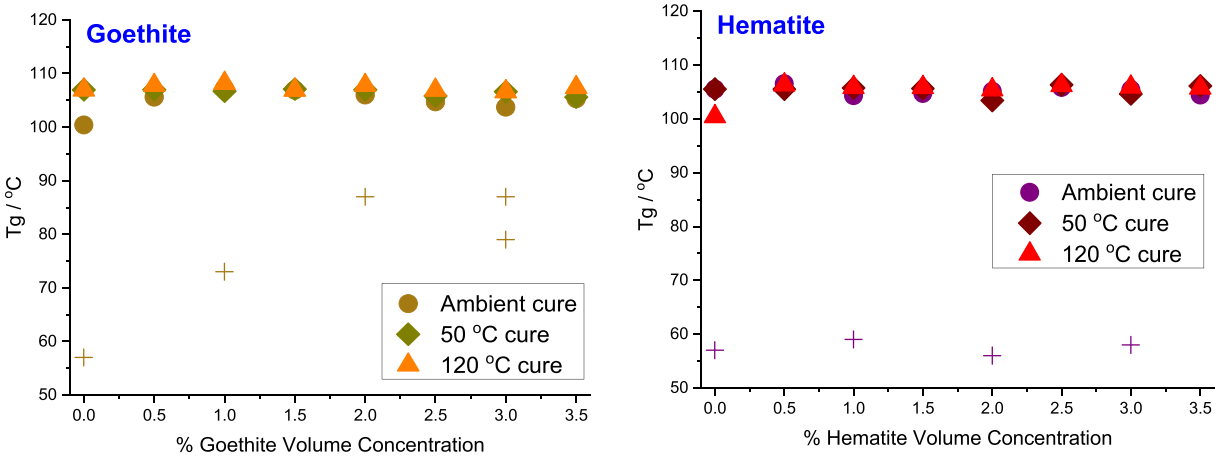

Fig. 5. Tg values obtained for stoichiometric DGEBA-MXDA resins cured for 7 days under ambient temperature followed by 2 h post-cure heating at 120 °C, 7 days at 50 °C under nitrogen followed by 2 h post-cure heating at 120 °C or 7 days at 120 °C under nitrogen, as a function of added goethite powder volume concentration (left) or added hematite powder volume concentration (right). The Tg values obtained for ambient cured DGEBA-TETA systems are represented as + points.

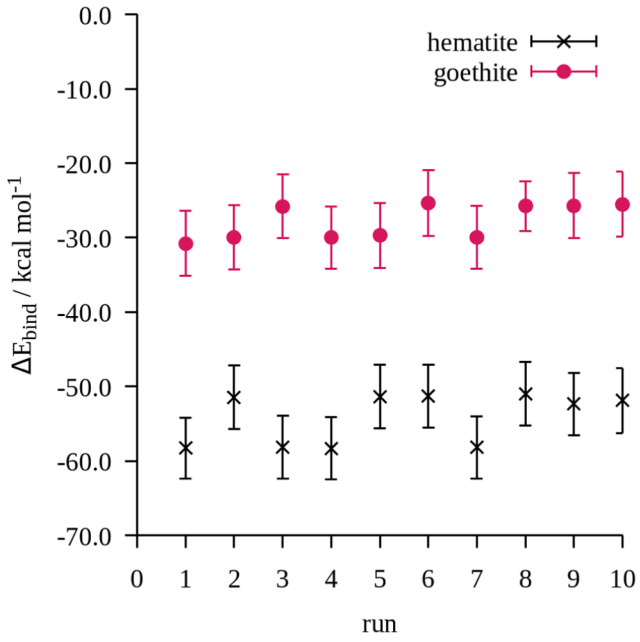

Fig. 6. Graph showing the binding energy for MXDA on hematite (black) and goethite (red) across 10 independent runs. The error bars correspond to the standard deviation for each run. (For interpretation of the references to colour in this figure legend, the reader is referred to the web version of this article.)

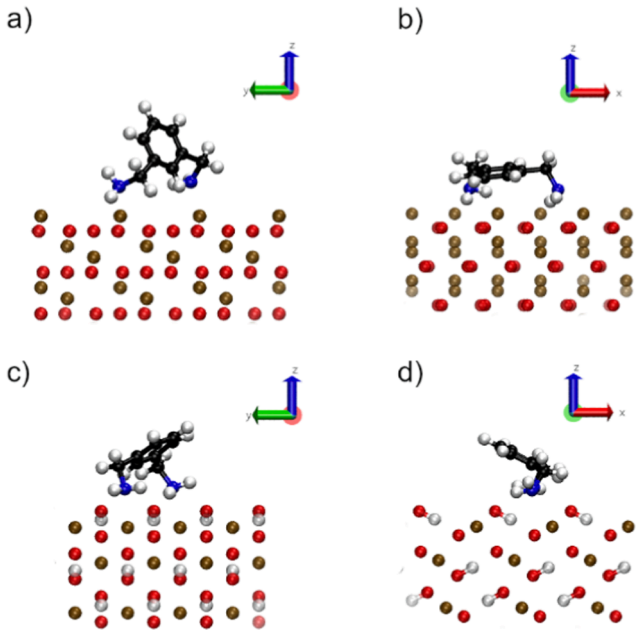

Fig. 7. Example snapshots of MXDA on a,b) hematite and c,d) goethite. A) and c) show the configurations with a higher $|r_{Aro-surface}|$ value, and b) and d) show an example from a lower $|r_{Aro-surface}|$.

the steric hindrance and repulsion between the δ- amine groups and oxygen atoms within the surface hydroxys.

The $|r_{N-N}|$ distances are also different for the two surfaces. On goethite, the $|r_{N-N}|$ are centred on 5.55 Å and 6.01 Å, which correspond to the distance between two Fe sites on the surface (See SI). However, on hematite the two groups are centred around 5.43 Å and 6.29 Å, which cannot be related to the underlying hexagonal lattice of Fe sites in the underlying crystal structure. These differences highlight the importance of the surface structure and the different binding mechanisms between

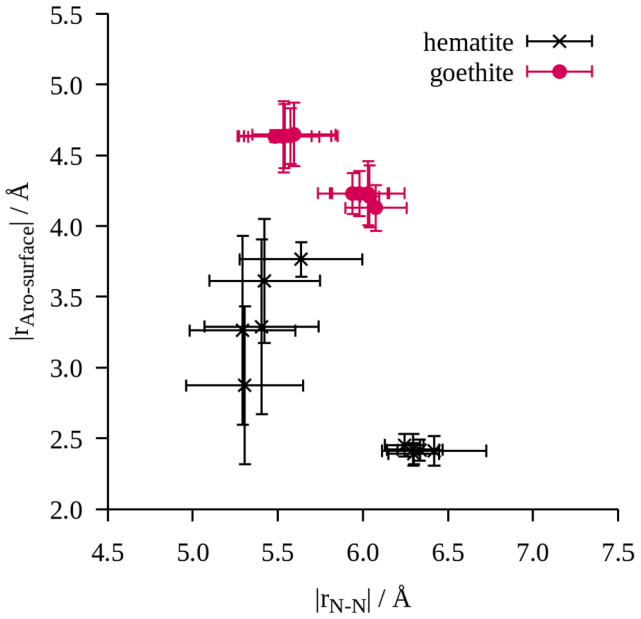

Fig. 8. Graph showing the distance between nitrogen atoms ($|r_{N-N}|$) and the distance between the aromatic ring and the surface ($|r_{Aro-surface}|$) for MXDA on hematite (black) and goethite (red) across 10 independent runs. The error bars correspond to the standard deviation for each run. (For interpretation of the references to colour in this figure legend, the reader is referred to the web version of this article.)

goethite and hematite that we previously reported on, in which electrostatic interactions dominate the binding to hematite, whilst goethite possesses the ability to form additional stabilizing hydrogen bond interactions.

The binding mode with the larger $|r_{N-N}|$ distance and smaller $|r_{Aro-surface}|$ corresponds to lower ΔE_{bind} values for both surfaces, due to the favourable interaction between the delocalised pi system on the aromatic ring and the surface (Fig. 9). There is an outlier in Fig. 9a on the hematite which has the largest $|r_{N-N}|$ separation and highest ΔE_{bind}, at 6.42 Å and −51.0 +/- 4.26 kcal mol^{-1} respectively.

Both the δ- nitrogen and the delocalised π-system in the benzene ring interact favourably with the δ + Fe sites on the surfaces, therefore ΔE_{bind} is more favourable when these interactions are maximised. We characterise the distance between the electronegative nitrogen in MXDA and the positive iron sites in the surface by calculating the radial distribution function (rdf), examples of which can be found in the SI. We fit a gaussian distribution to the first peak to extract the distance between the nitrogen and iron, shown in Fig. 10. In all cases, the first peak on hematite is closer than goethite, due in part to the definition of the surface mentioned earlier, but also due to the structure of the surface. In goethite, there are hydroxy groups above the δ + Fe which obstruct the nitrogen from the δ + Fe sites, whilst simultaneously stabilising the binding mode through additional hydrogen bonds.

Fig. 10 shows that the position of the first peak and the $|r_{Aro-surface}|$ show the opposite trends with the two surfaces. That is, for hematite the position of the first peak in the rdf is at a longer distance for the less upright binding mode, whilst for goethite the position of the first peak in the rdf is at a shorter distance for the less upright binding mode. This difference exemplifies the different surface characteristics. In goethite the δ + Fe are isolated sites, whilst hematite has a more diffuse δ + surface. Therefore, for goethite stronger *N*-Fe binding is observed which follows the underlying surface structure, whilst for hematite multiple weaker *N*-Fe interactions are formed.

The colour bar in Fig. 10 indicates ΔE_{bind}, and for goethite the lower energy binding mode has the rdf first peak position around 2.55–2.60 Å and $|r_{Aro-surface}| \approx 4.2$ Å, whist the slightly higher energy binding mode

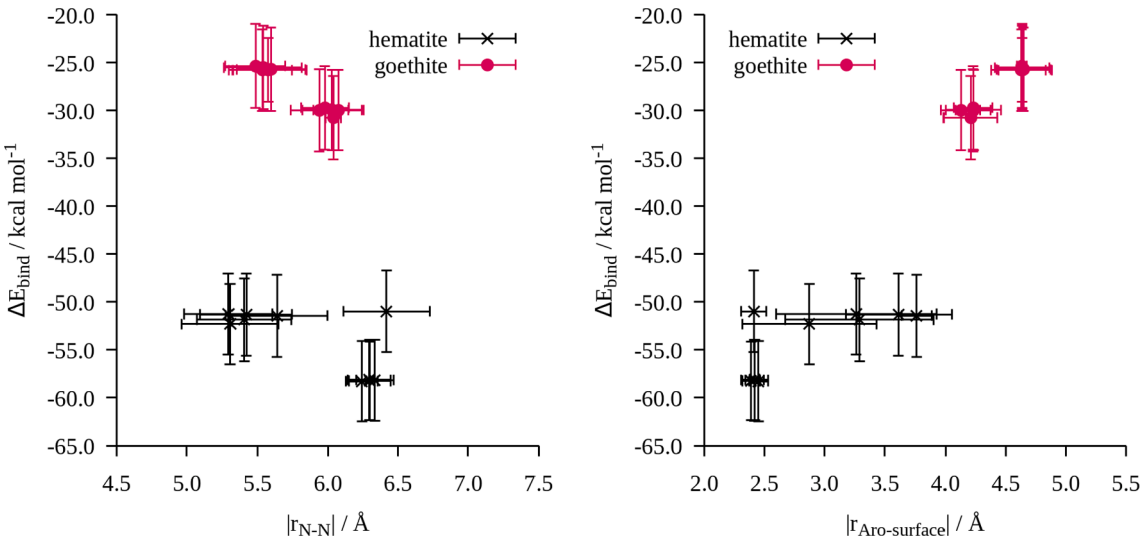

Fig. 9. Graph showing the binding energy as a function of (a) distance between nitrogen atoms ($|r_{N-N}|$) and (b) the distance between the aromatic ring and the surface ($|r_{Aro-surface}|$) for MXDA on hematite (black) and goethite (red) across 10 independent runs. The error bars correspond to the standard deviation for each run. (For interpretation of the references to colour in this figure legend, the reader is referred to the web version of this article.)

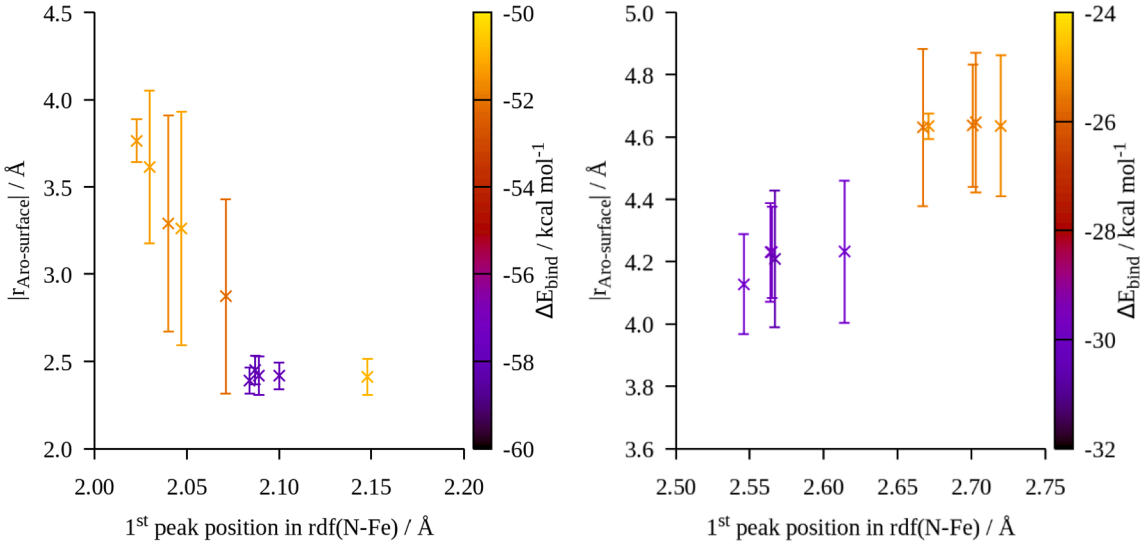

Fig. 10. Graph showing the position of the first peak in the rdf and distance between the aromatic ring and the surface ($|r_{Aro-surface}|$) for MXDA on (a) hematite and (b) goethite across 10 independent runs. The error bars correspond to the standard deviation for each run. The colour bar corresponds to the binding energy.

has the first peak position in the rdf at around 2.65–2.75 Å and $|r_{Aro-surface}| \approx 4.8$ Å.For hematite the lower energy binding mode has a well resolved first peak at approximately 2.08 Å, and $|r_{Aro-surface}| \approx 2.4$ Å. The higher energy binding mode, however, shows a distribution of $|r_{Aro-surface}|$ and rdf first peak positions, indicated by the yellow/orange points in Fig. 10 (left). Upon closer inspection of the simulations, this is due to the MXDA molecule switching between the two binding modes, which can be observed by monitoring $|r_{Aro-surface}|$ as a function of time throughout the simulation. This switching between states was not observed for the goethite surface and explains why in Fig. 10 the modes are more resolved. Indeed, for a single simulation of 20 ns (after the initial 4 ns equilibration period) we only see one switch from the slightly higher binding mode to the lower one for goethite, whilst for hematite we see several switches between binding modes over the 4 ns production runs (Fig. 11). The difference in switching behaviour observed indicates that the energy barrier for switching lower for hematite than goethite.

We have compared the binding of MXDA to our previous study of TETA. We found two clusters of $|r_{N-N}|$ at approximately 5 Å and 8 Å, however these have very similar ΔE_{bind} values for TETA on hematite. On goethite we find two values for ΔE_{bind} separated by 5 kcal mol^{-1} as for MXDA, however this is not resolved into two groups based on $|r_{N-N}|$, although we observe the strong site-specific binding motif with the TETA forming a bridging conformation in all simulations on goethite. These results were found through additional simulations and analogous measurements for the two terminal primary amine groups in TETA and can be found in the SI.

5. Discussion

It has been proposed that under-cured regions developed independently of the surface binding in epoxy-amine resins, as a result of entropic segregation of smaller, more flexible molecules during the cure. Previously, infrared characterisation of DGEBA-TETA/iron oxide composite systems indicated that the chemical interphase was comprised of partially reacted polymer, with detectable levels of residual epoxy [16].

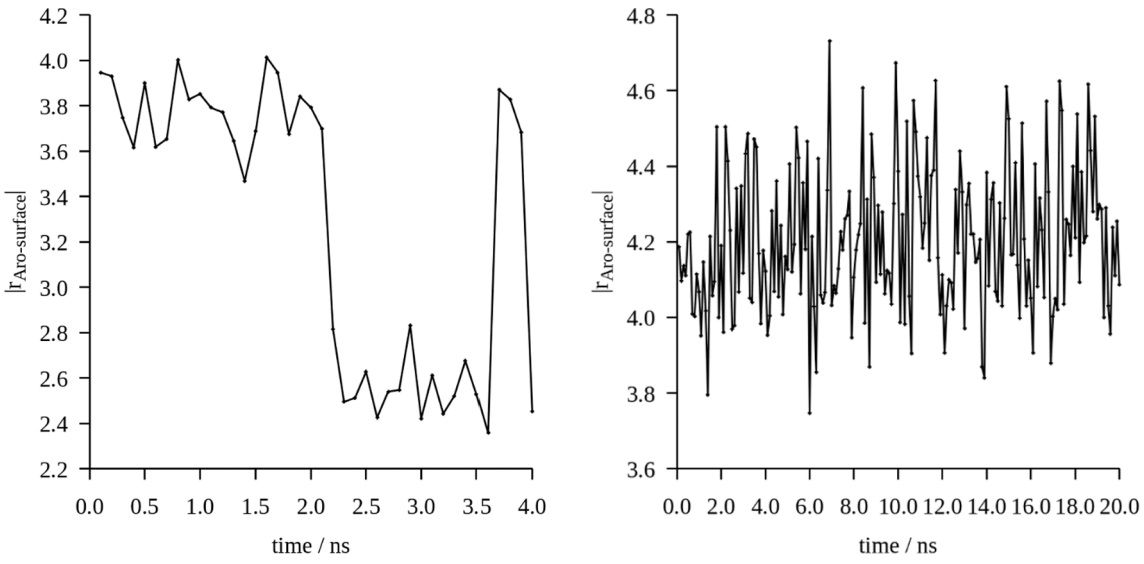

Fig. 11. Graph showing the distance between the aromatic ring and the surface ($|r_{Aro-surface}|$) for MXDA on (a) hematite and (b) goethite through time for one representative run.

The more detailed analysis presented here for DGEBA-MXDA composites also supports this hypothesis, since under-curing occurs to a similar extent in both hematite and goethite composite specimens after reaction under ambient temperature, despite the differences in chemistry, binding modes and energies calculated by molecular dynamic simulations. This hypothesis is also in keeping with recently published full-atomistic molecular dynamics simulations showing that entropic segregation at a neutral surface will occur according to the size and flexibility of molecules, and this produces chemical gradients in cured epoxy-amine polymers [44]. An additional key finding of the present study however, is that amine adsorption occurs and persists during and after the cross-linking reaction, displaying different temperature dependencies to entropic effects. According to reported simulations and thermodynamic considerations, this is expected to yield residual amine depletion in the interphase at the nanoscale [45,46].

Molecular dynamics simulations provided evidence that the primary amine groups of MXDA bind strongly to goethite surfaces via synergistic hydrogen bonding between surface hydroxy groups and the electrostatic interactions between the amine group and iron. In the case of TETA and DGEBA molecules studied previously, this phenomenon was reflected in the adoption of immobilised, upright, energetically unfavourable "bridging" conformations protruding into vacuum, to access specific binding sites [16]. Here, MXDA is also shown to adopt more upright conformation on goethite, whilst the distance between the two amine nitrogen atoms mirrors the underlying lattice spacing, further supporting this hypothesis. Over the last 4 ns of the simulation run we calculated the number of hydrogen bonds in which the amine group on the MXDA is the donor, taking configurations every 0.1 ns. We found that for goethite there was on average 0.76 hydrogen bonds, whilst on hematite there were significantly fewer, with an average of 0.13 (See SI for more details). In addition, the energy barrier to switching between the two newly identified binding modes is higher on goethite than hematite, due to strong site-specific binding. The simulation results are thus consistent with the cure-temperature dependence of residual amine concentration in composites, where stronger adsorption to goethite is proposed to prevent activated desorption occurring on hematite during reaction at 50 °C and 120 °C.

Finally, taken together with our previous results and the molecular dynamics simulations reported here, the absence of a Tg shift for DGEBA-MXDA composites sheds further light on the establishment of binding between epoxy-amine networks and goethite. In the case of DGEBA-TETA cross-linked networks, molecular dynamics simulations indicated that adsorbed DGEBA epoxy molecules, TETA amine molecules and tertiary amine molecules based on the cross-linked junction all exhibited energetically unfavourable bridging conformations extending into the vacuum on goethite; indicating strong binding through the peripheral primary amine (TETA) or hydroxy (DGEBA and tertiary amine) groups [16]. However, whilst TETA adsorption was the most energetically favourable of the three molecules investigated, it remained unclear whether (i) during the cure TETA binding was followed by reaction of the two unbound secondary amine groups, and hence the incorporation of the bound TETA molecule into the network, or (ii) amine adsorption was dynamic during network formation, and strong binding with the network occurred through secondary hydroxy generated near cross-link junctions. Molecular dynamics simulations here demonstrated that for MXDA diamine cross-linkers, all the available amine groups are involved in molecular surface binding to goethite, rendering the molecule unavailable for incorporation into the network, thus negating the first possibility, Scheme 2. On the other hand, the position of secondary hydroxy molecules near to the cross-link junction in is similar in DGEBA-MXDA resins, so that oligomer or polymer-surface binding could feasibly proceed in a similar manner. Since DGEBA-MXDA resins show no Tg dependency, this second possibility can be discounted and we can conclude that polymer dynamics are primarily dictated by the preferential adsorption and further reaction of amine molecules, Scheme 2.

6. Conclusions

We have employed a holistic approach coupling molecular simulations with FTIR and DSC techniques to investigate the influence of cross-linker topology on epoxy resin/iron oxide composites. We have compared the binding of m-xylylenediamine (MXDA) to previously reported results using triethylenetetraamine (TETA) to elucidate the polymer network – goethite binding mechanism in the case of epoxy-amine resins and compare it to the binding mechanism in hematite. We find strong site-specific binding on a goethite surface for both cross-linkers through the terminal amine groups. In the case of MXDA we find that the Tg has no dependence on the pigment volume concentration, unlike the case of TETA. In addition, from molecular dynamics simulations we find that MXDA has two low-energy binding modes due to the increased rigidity of the cross-linker over TETA. The energy barrier for interconversion between the two modes is higher for goethite than hematite. From these results we propose that network polymer dynamics

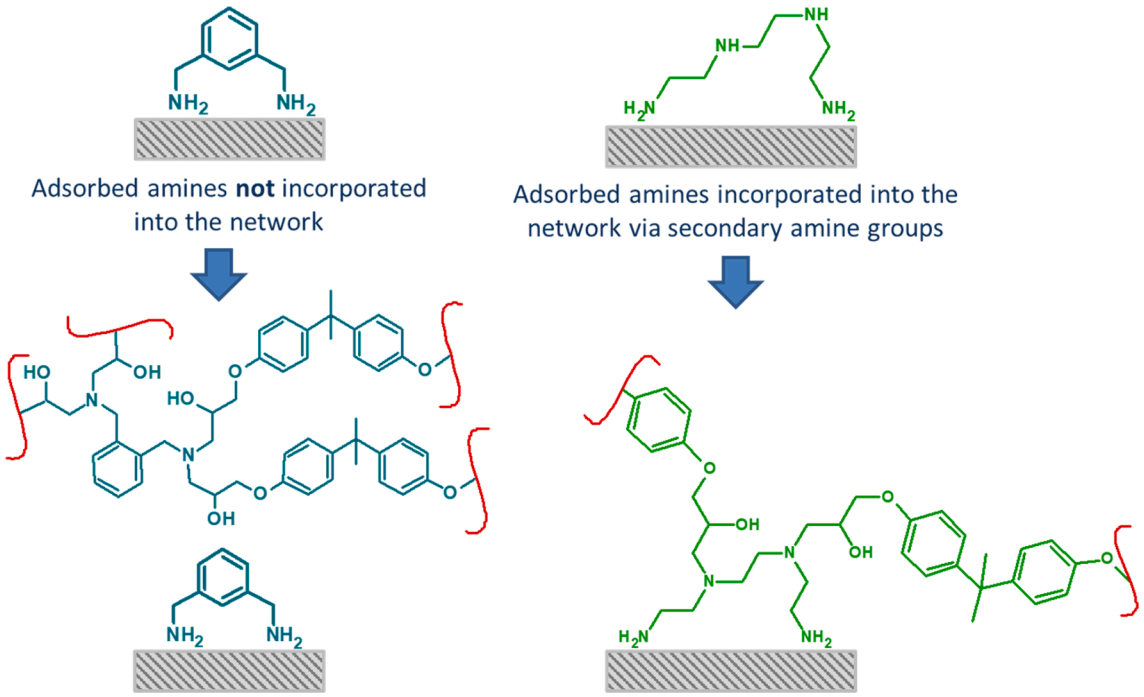

Scheme 2. Illustration of the proposed adsorption of MXDA onto goethite occurring separately to network formation (left), and the adsorption of TETA followed by its incorporation into the epoxy network through reaction of central secondary amine groups.

may be restricted in the case of strong site-specific binding, as in the case of goethite, but that this only occurs when the cross-linker topology allows the bound molecule to be incorporated into the resin, e.g., through secondary amines present in TETA. This has implications in the formulation and design of epoxy resin composites, adhesives, and protective coatings.

CRediT authorship contribution statement

Suzanne Morsch: Conceptualization, Methodology, Formal analysis, Investigation, Writing – original draft. **Charlie R. Wand:** Conceptualization, Methodology, Formal analysis, Investigation, Writing – original draft. **Simon Gibbon:** Writing – review & editing, Funding acquisition. **Mark Irwin:** Writing – review & editing, Supervision, Project administration. **Flor Siperstein:** Writing – review & editing, Supervision, Project administration. **Stuart Lyon:** Writing – review & editing, Supervision, Funding acquisition, Project administration.

Declaration of Competing Interest

The authors declare that they have no known competing financial interests or personal relationships that could have appeared to influence the work reported in this paper.

Data availability

Data will be made available on request.

Acknowledgements

S. Morsch and C. R. Wand acknowledge AkzoNobel, and the EPSRC (grant number EP/S004963/1) for materials and financial support. C. R. Wand and F. Siperstein would like to acknowledge the assistance given by Research IT and the use of the Computational Shared Facility at The University of Manchester.

Appendix A. Supplementary material

Supplementary data to this article can be found online at https://doi.org/10.1016/j.apsusc.2022.155380.

References

[1] G.R. Palmese, R.L. McCullough, N.R. Sottos, Relationship between interphase composition, materials properties, and residual thermal stresses in composite materials, J. Adhes. 52 (1995) 101–113.
[2] H. Yim, M. Kent, W.F. McNamara, R. Ivkov, S. Satija, J. Majewski, Structure within thin epoxy films revealed by solvent swelling: a neutron reflectivity study, Macromolecules 32 (1999) 7932–7938.
[3] I.A. Starostina, D.A. Nguyen, E.V. Burdova, O.V. Stoyanov, Adhesion of polymers: new approaches to determination of surface properties of metals, Polym. Sci., Ser. D 6 (2013) 1–4.
[4] A.A. Roche, M. Aufray, J. Bouchet, The role of the residual stresses of the epoxy-aluminum interphase on the interfacial fracture toughness, J. Adhes. 82 (2006) 867–886.
[5] S. Morsch, Y. Liu, M. Malanin, P. Formanek, K.-J. Eichhorn, Exploring whether a buried nanoscale interphase exists within epoxy-amine coatings: implications for adhesion, fracture toughness, and corrosion resistance, ACS Appl. Nano Mater. 2 (2019) 2494–2502.
[6] S.G.R. Emad, X. Zhou, S.B. Lyon, G.E. Thompson, Y. Liu, G. Smyth, D. Graham, D. Francis, S.R. Gibbon, Influence of volume concentration of active inhibitor on microstructure and leaching behaviour of a model primer, Prog. Org. Coat. 102 (2017) 71–81.
[7] J. Bouchet, A.-A. Roche, The formation of epoxy/metal interphases: mechanisms and their role in practical adhesion, J. Adhes. 78 (2002) 799–830.
[8] S. Bentadjine, R. Petiaud, A.A. Roche, V. Massardier, Organo-metallic complex characterization formed when liquid epoxy-diamine mixtures are applied onto metallic substrates, Polymer 42 (2001) 6271–6282.
[9] M. Aufray, A. André Roche, Epoxy-amine/metal interphases: influences from sharp needle-like crystal formation, Int. J. Adhes. Adhes. 27 (2007) 387–393.
[10] C. Wehlack, W. Possart, J.K. Krüger, U. Müller, Epoxy and polyurethane networks in thin films on metals—formation, structure properties, Soft Mater. 5 (2007) 87–134.
[11] C. Wehlack, W. Possart, Characterization of the epoxy-metal interphase: FTIR-ERAS and spectra calculation for ultra-thin films, Macromol. Symp. 205 (2004) 251–261.
[12] S.N. Goyanes, F. Saavedra, A.J. Roncaglia, G.H. Rubiolo, Variation in physical and mechanical properties with coating thickness in epoxy-diamine-aluminum system, J. Appl. Polym. Sci. 98 (2005) 891–895.
[13] A. Meiser, W. Possart, Epoxy-metal interphases: chemical and mechanical aging, J. Adhes. 87 (2011) 313–330.

[14] P. Taheri, H. Terryn, J.M.C. Mol, Applied surface science An in situ study of amine and amide molecular interaction on Fe surfaces, Appl. Surf. Sci. 354 (2015) 242–249.
[15] B. Salgin, Ö. Özkanat, J.M.C. Mol, H. Terryn, M. Rohwerder, Role of surface oxide properties on the aluminum/epoxy interfacial bonding, J. Phys. Chem. C 117 (2013) 4480–4487.
[16] S. Morsch, C.R. Wand, S. Emad, S. Lyon, F. Siperstein, M. Malanin, J. Muche, A. Caspari, A. Drechsler, K.-J. Eichhorn, S. Gibbon, Molecular origins of epoxy-amine/iron oxide interphase formation, J. Colloid Interface Sci. 613 (2022) 415–425.
[17] P. Rittigstein, R.D. Priestley, L.J. Broadbelt, J.M. Torkelson, Model polymer nanocomposites provide an understanding of confinement effects in real nanocomposites, Nat. Mater. 6 (2007) 278–282.
[18] T. Semoto, Y. Tsuji, K. Yoshizawa, Molecular understanding of the adhesive force between a metal oxide surface and an epoxy resin, J. Phys. Chem. C 115 (2011) 11701–11708.
[19] J.M. Knaup, C. Köhler, T. Frauenheim, A.T. Blumenau, M. Amkreutz, P. Schiffels, B. Schneider, O.D. Hennemann, Computational studies on polymer adhesion at the surface of γ-Al 2O3. I. The adsorption of adhesive component molecules from the gas phase, J. Phys. Chem. B 110 (2006) 20460–20468.
[20] K. Yoshizawa, H. Murata, H. Tanaka, Density-functional tight-binding study on the effects of interfacial water in the adhesion force between epoxy resin and alumina surface, Langmuir 34 (2018) 14428–14438.
[21] J.H. Lee, S.G. Kang, Y. Choe, S.G. Lee, Mechanism of adhesion of the Diglycidyl Ether of Bisphenol A (DGEBA) to the Fe(100) surface, Compos. Sci. Technol. 126 (2016) 9–16.
[22] J.H. Lee, Y. Choe, S.G. Lee, Adhesion mechanism of bisphenol A diglycidyl ether (BADGE) on an α-Fe_2O_3 (0001) surface, J. Ind. Eng. Chem. 53 (2017) 62–67.
[23] G. Bahlakeh, M. Ghaffari, M.R. Saeb, B. Ramezanzadeh, F. De Proft, H. Terryn, A close-up of the effect of iron oxide type on the interfacial interaction between epoxy and carbon steel: combined molecular dynamics simulations and quantum mechanics, J. Phys. Chem. C 120 (2016) 11014–11026.
[24] M.J. Marks, R.V. Snelgrove, Effect of conversion on the structure-property relationships of amine-cured epoxy thermosets, ACS Appl. Mater. Interfaces 1 (2009) 921–926.
[25] N.J. Jin, J. Yeon, I. Seung, K.S. Yeon, Effects of curing temperature and hardener type on the mechanical properties of bisphenol F-type epoxy resin concrete, Constr. Build. Mater. 156 (2017) 933–943.
[26] C.R. Wand, S. Gibbon, F.R. Siperstein, Adsorption of epoxy oligomers on iron oxide surfaces: the importance of surface treatment and the role of entropy, Langmuir 37 (2021) 12409–12418.
[27] S. Plimpton, Fast parallel algorithms for short-range molecular dynamics, J. Comput. Phys. 117 (1995) 1–19.
[28] S. Nosé, A unified formulation of the constant temperature molecular dynamics methods, J. Chem. Phys. 81 (1984) 511–519.
[29] L.C. Verlet, "Experiments" on classical fluids. I. Thermodynamical properties of lennard-jones molecules, J. Phys. D: Appl. Phys. 159 (1967) 98–103.
[30] R.W. Hockney, J.W. Eastwood, Computer Simulation using Particles, CRC Publisher, 1988.
[31] L.W. Finger, R.M. Hazen, Crystal structure and isothermal compression of Fe_2O_3, Cr_2O_3, and V_2O_5 to 50 Kbars, J. Appl. Phys. 51 (1980) 5362–5367.
[32] A.F. Gualtieri, P. Venturelli, In situ study of the goethite-hematite phase transformation by real time synchrotron powder diffraction, Am. Mineral. 84 (1999) 895–904.
[33] R.T. Cygan, J.J. Liang, A.G. Kalinichev, Molecular models of hydroxide, oxyhydroxide, and clay phases and the development of a general force field, J. Phys. Chem. B 108 (2004) 1255–1266.
[34] S. Kerisit, Water structure at hematite-water interfaces, Geochim. Cosmochim. Acta 75 (8) (2011) 2043–2061.
[35] J.P. Ryckaert, G. Ciccotti, H.J.C. Berendsen, Numerical integration of the cartesian equations of motion of a system with constraints: molecular dynamics of n-alkanes, J. Comput. Phys. 23 (1977) 327–341.
[36] L.S. Dodda, J.Z. Vilseck, J. Tirado-Rives, W.L. Jorgensen, 1.14*CM1A-LBCC: localized bond-charge corrected CM1A charges for condensed-phase simulations, J. Phys. Chem. B 121 (2017) 3864–3870.
[37] L.S. Dodda, I.C. De Vaca, J. Tirado-Rives, W.L. Jorgensen, LigParGen web server: an automatic OPLS-AA parameter generator for organic ligands, Nucl. Acids Res. 45 (2017) W331–W336.
[38] A.I. Jewett, Z. Zhuang, J.-E. Shea, Moltemplate a coarse-grained model assembly tool, Biophys. J. 104 (2) (2013) 169a.
[39] N. Michoud-Agrawal, E.J. Denning, T.B. Woolf, O. Beckstein, MDAnalysis: a toolkit for the analysis of molecular dynamics simulations, J. Comput. Chem. 32 (2011) 2319–2327.
[40] Gowers, R.; Linke, M.; Barnoud, J.; Reddy, T.; Melo, M.; Seyler, S.; Domański, J.; Dotson, D.; Buchoux, S.; Kenney, I.; Beckstein, O. MDAnalysis: A Python Package for the Rapid Analysis of Molecular Dynamics Simulations. *Proc. 15th Python Sci. Conf.* **2016**, 98–105.
[41] S. Morsch, Y. Liu, S.B. Lyon, S.R. Gibbon, Insights into epoxy network nanostructural heterogeneity using AFM-IR, ACS Appl. Mater. Interfaces 8 (2016) 959–966.
[42] S. Morsch, Z. Kefallinou, S. Gibbon, Y. Liu, B. Lyon, S., Controlling the nanostructure of epoxy resins: reaction selectivity and stoichiometry, Polymer 143 (2018) 10–18.
[43] S. Morsch, Y. Liu, P. Greensmith, S.B. Lyon, S.R. Gibbon, Molecularly controlled Epoxy network nanostructures, Polymer 108 (2017) 146–153.
[44] S. Yamamoto, K. Tanaka, Entropy-driven segregation in epoxy-amine systems at a copper interface, Soft Matter 17 (5) (2021) 1359–1367.
[45] M. Langeloth, T. Sugii, M.C. Böhm, F. Müller-Plathe, Formation of the interphase of a cured epoxy resin near a metal surface: reactive coarse-grained molecular dynamics simulations, Soft Mater. 12 (2014) S71–S79.
[46] G.R. Palmese, R.L. McCullough, Kinetic and thermodynamic considerations regarding interphase formation in thermosetting composite systems, J. Adhes. 44 (1994) 29–49.